ELSEVIER

Journal of Crystal Growth 157 (1995) 386–391

JOURNAL OF CRYSTAL GROWTH

Optical and electronic properties of SiGeC alloys grown on Si substrates

J. Kolodzey [a,*], P.R. Berger [a], B.A. Orner [a], D. Hits [a], F. Chen [a], A Khan [a], X. Shao [a], M.M. Waite [b], S. Ismat Shah [b], C.P. Swann [c], K.M. Unruh [c]

[a] *Department of Electrical Engineering, University of Delaware, 140 Evans Hall, Newark, Delaware 19716, USA*

[b] *Dupont Experimental Station, P.O. Box 80356, Wilmington, Delaware 19898, USA*

[c] *Department of Physics and Astronomy, University of Delaware, Newark, Delaware 19716, USA*

Abstract

Metastable $Si_{1-x-y}Ge_xC_y$ alloys were grown by molecular beam epitaxy on (100) Si substrates. Solid elemental sources were used for the Si and Ge beams, and a resistively heated graphite filament was used for the C beam. Up to 3 at% of C was incorporated in the alloy layers. Optical transmission measurements showed that the absorption edge of thick layers increased to higher energies with increasing C fraction, and revealed the presence of Si–C and Ge–C vibrational modes in the infrared. At low temperatures, the alloys showed significant photoluminescence. The bandgap energies of thick layers increased linearly with the C fraction and followed a linear dependence of the bandgap on composition. Measurements of the valence band density of states using X-ray photoelectron spectroscopy indicated that the valence band energy maximum increased with the C fraction relative to that of SiGe alloys of similar composition. Our results indicated that SiGeC alloys are promising materials for Si-based heterostructure devices.

1. Introduction

Recently, alloys of the Group IV elements have become interesting for heterostructure devices compatible with Si integrated circuit technology. Research has been challenged by the low equilibrium solid solubility of C in Si and in Ge, but metastable $Si_{1-x-y}Ge_xC_y$ alloys with significant C atomic fractions have been grown by non-equilibrium techniques such as molecular beam epitaxy (MBE) [1] and chemical vapor deposition [2]. Although the equilibrium solubility of C is 10^{-6} in Si [3], and is 10^{-14} in Ge [4], we have incorporated up to 3 at% of C under the non-equilibrium growth conditions of MBE. These alloys were solid solutions with a diamond cubic structure as indicated by X-ray diffraction [5]. An intriguing possibility is that the lattice constant of these alloys can be matched to that of Si by adjusting the composition ratios. In addition, the bandgap might be tunable to match desired optical wavelengths. The availability of optoelectronic heterostructures compatible with Si circuits would have a major impact on practical applications including microprocessors having monolithically integrated optical input/output channels [6].

Recent studies have focused on alloy growth conditions, structure, composition and luminescence [7–9]. Numerical values for physical properties and their dependence on composition are becoming more well known. Interpretation of alloy properties has been complicated by the effects of strain and by structural

* Corresponding author. Fax: +1 302 831 4316.

0022-0248/95/$09.50 © 1995 Elsevier Science B.V. All rights reserved
SSDI 0022-0248(95)00329-0

defects. Strain can reduce the bandgap energy, which is opposite to the alloying effect of adding C which increases the bandgap energy. The small atomic size of C relative to Si and Ge creates local strain and a locally distorted lattice. Therefore SiGeC alloys may behave as a new material with its own degree of strain [10].

In this work we describe the growth and properties of metastable random alloys of SiGeC. The alloys were grown by molecular beam epitaxy (MBE) using solid elemental sources, and the properties were measured by several analytical techniques. The alloys had a diamond cubic structure and the bandgap energy of thick layers depended linearly on composition.

2. The deposition system

Growth was performed in an EPI 620 MBE system comprising a growth chamber and a specimen introduction chamber. The growth chamber had six effusion cell ports and was equipped with reflection high energy electron diffraction (RHEED), optical pyrometry for substrate temperature measurement, and a quadrupole mass analyzer for residual gas analysis (RGA). The growth chamber was evacuated by a 400 l/s ion pump and a 1 500 l/s cryopump, achieving a base pressure of 4×10^{-9} Pa. Panels in the growth temperature contained a circulating mixture of ethylene glycol and water to adsorb background gases, and to cool effusion cells and the substrate manipulator.

The Si source used float-zone refined intrinsic Si in a novel crucible of TiB_2 ceramic coated on the outside with W metal [11]. Using a high temperature effusion cell, the Si growth rate was 0.1 μm/h at 1850°C. Above 1900°C, the TiB_2 ceramic began to decompose and small amounts of Ti and B impurities were incorporated into the alloy layers, as shown by secondary ion mass spectrometry (SIMS).

The Ge source was triple zone-refined polycrystalline Ge loaded into a pyrolytic boron nitride crucible. Using a standard temperature effusion cell, the Ge growth rate was 0.07 μm/h at 1350°C. The Ge cell temperature was kept below 1400°C to avoid leaching B from the crucible and contaminating the Ge melt.

The C source was an electrical filament machined from pyrolytic graphite (PG), heated by applying a direct current. Only W metal and graphite were used near the C evaporation hot zone in the cell. Two types of PG with different purity levels were investigated, and the higher purity PG produced less CO and CO_2 (the principal impurities) during outgassing. RGA analysts showed that C_3 was the principal pure C molecule that was evaporated. At a filament current of 38 A, the effective C growth rate was 0.01 μm/h at a filament temperature of 2030°C.

The substrates were 75 mm diameter, (100) oriented Si wafers. The wafers were degreased, etched in $H_2O:H_2O_2:HCl$ (5 : 3 : 3), followed by $HF:H_2O$ (1 : 10), and loaded into the introduction chamber[12]. In the growth chamber, substrates were outgassed at 250°C for 60 min. Substrate growth temperatures ranged from 400 to 600°C.

3. Alloy characterization

Film thicknesses were measured by optical interference and by stylus profilometry. For the C growth rate, we estimated an effective incorporation growth rate from the change in thickness of the alloys compared to pure Ge films grown under similar conditions. Transmission electron microscopy (TEM) indicated the crystal quality. X-ray diffraction was measured with a single crystal θ–2θ diffractometer using Cu Kα radiation to determine the alloy structure. The SiGeC alloy films grown at 400°C had a polycrystalline diamond cubic structure with the (110) planes preferentially oriented parallel to the (100) Si substrate. GeC binary alloys grown at 600°C had a single crystal (100) diamond cubic structure oriented to the substrate. Applying Bragg's Law to the diffracted intensity peaks yielded the lattice constants.

Compositions were measured by Auger electron spectroscopy (AES), Rutherford backscattering spectrometry (RBS), SIMS, and by X-ray photoelectron spectroscopy (XPS). Prior to measurements, the surfaces were ion-sputtered until no surface oxygen was detectable. The fine structure of the Auger KLL signals indicated that the C formed sp^3 bonds with neighboring atoms [13].

The optical absorbance was measured over a range

of wavelengths from the near to the far infrared (IR) by Fourier transform infrared spectroscopy (FTIR) in the transmission mode. Far IR absorption indicated infrared-active vibrational modes from Si–Ge, Si–C, and Ge–C. Near IR measurements yielded the optical absorption edge and the bandgap. Photoluminescence (PL) spectra were collected using a 1 m grating spectrometer with a liquid nitrogen-cooled Ge detector. Excitation was by a multi-line Ar ion laser operating at wavelengths of 488 and 514 nm, with a total laser beam power of 120 mW which was filtered and then focused to a 2 mm diameter spot. The samples were mounted in a liquid He cryostat for low temperature measurements.

XPS measurements yielded the valence band density of states in addition to the composition. From the energy of the valence band edge, it was possible to obtain the relative valence band offset energies versus composition which are important for heterostructure design. The conduction band offsets could then be inferred from the values for valence band offsets and the bandgap energies.

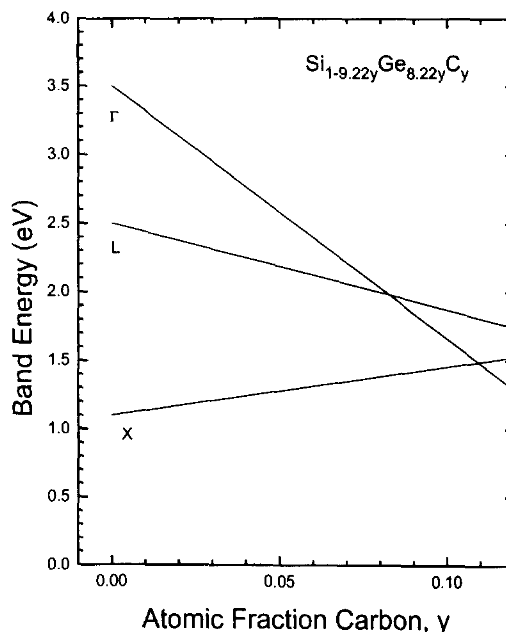

Fig. 2. Theoretical energies of conduction band minima based on linear interpolation from known Si, Ge and C endpoint values. This set of composition values was predicted to be lattice-matched to Si.

4. Results and discussion

4.1. Crystalline structure

X-ray diffraction showed intensity peaks corresponding to a diamond cubic lattice structure. Fig. 1 shows a typical plot of X-ray diffracted intensity versus diffraction angle for a $Ge_{1-y}C_y$ alloy. Samples grown at 400°C had a polycrystalline structure with the (110) planes preferentially oriented to the (001) Si substrate. Samples grown at 600°C had (001) planes oriented parallel to the substrate. There was, however, a possibility of (001) plane grains being misoriented by an angle about the [001] growth direction. This was consistent with TEM measurements which showed twins and stacking faults at the alloy/substrate interface.

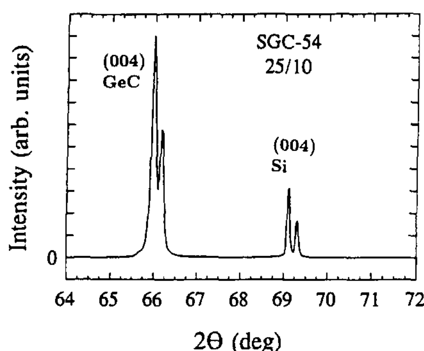

Fig. 1. X-ray diffraction intensity versus diffraction angle for a $Ge_{0.98}C_{0.02}$ alloy, showing reflections from the (004) lattice planes of the alloy at $2\theta = 66°$ and of the Si substrate at $2\theta = 69.2°$. Peak angles positions indicate a diamond cubic structure and the value for the lattice constant.

4.2. Dependence of bandgap on composition

Strain can reduce the bandgap of thin pseudomorphic alloy layers [14], and therefore we have investigated thick layers in order to obtain bulk values for the bandgap versus composition. Using tabulated band energies of pure Si, Ge, and C as the endpoints [15], Fig. 2 gives linearly interpolated theoretical values for the Γ ([000]), L ([111]), and X ([100]) conduction band minima with respect to the valence band maximum for the range of composition values, $Si_{1-9.22y}Ge_{8.22y}C_y$, predicted to be lattice-matched

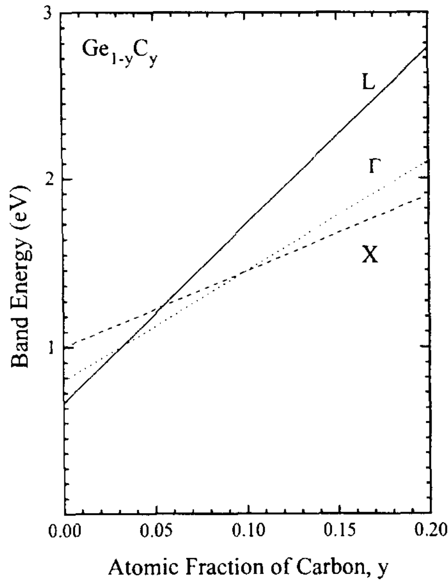

Fig. 3. Theoretical energies of the conduction band minima of binary $Ge_{1-y}C_y$ alloys, based on a linear interpolation.

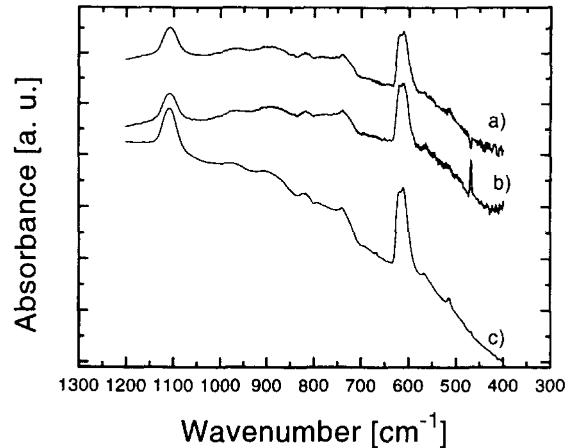

Fig. 4. Infrared absorbance versus photon wavenumber for $Si_{0.08}Ge_{0.90}C_{0.02}$ (top, a) and $Si_{0.08}Ge_{0.91}C_{0.01}$ (center, b) compared with pure Ge (bottom, c).

to Si substrates. It is interesting that for the maximum value of $y = 0.11$, significant numbers of electrons may occupy both the X and the Γ valleys.

Fig. 3 shows theoretical band energies for binary $Ge_{1-y}C_y$ alloys. This binary alloy is lattice matched to Si only for $y = 0.11$, but the linear interpolation predicts the bandgap to be direct in k space for C atomic fractions $0.04 \leq y \leq 0.11$. The possibilities of direct bandgap Group IV semiconductors should have profound consequences for optical devices.

Table 1
Measured properties including sample number, composition, lattice constant a, bandgap E_g, and layer thickness t measured by optical interference; the calculated minimum bandgaps, E_g(calc), were determined by linear interpolation versus composition of the Γ,X, and L bands (as in Fig. 2), are for comparison; T_{sub} is the substrate growth temperature

Sample	Composition	a (nm)	E_g (eV)	t (μm)	E_g(calc) (eV)	T_{sub} (°C)
SGC-19	$Si_{0.08}Ge_{0.90}C_{0.02}$	0.56348	1.046	0.49	1.041	400
SGC-20	$Si_{0.08}Ge_{0.91}C_{0.01}$	0.56394	0.991	0.47	0.956	400
SGC-30	$Ge_{0.99}C_{0.01}$	0.56544	0.732	0.582	-	600
SGC-31	$Ge_{0.98}C_{0.02}$	0.56539	0.782	0.139	-	600
SGC-32	$Ge_{0.97}C_{0.03}$	0.56525	0.875	0.136	-	600

The experimental bandgaps of the SiGeC alloys were measured by two techniques: optical absorption and PL. From optical absorption, the bandgap was estimated from the energy at which the optical absorption coefficient $\alpha = 5$ cm^{-1}. Table 1 gives the properties of several $Si_{1-x-y}Ge_xC_y$ alloys versus composition. Fig. 4 shows a plot of infrared absorbance versus photon wavenumber for samples of SiGeC. Absorption at 604 cm^{-1} is attributed to the localized vibrational mode of C in Si and to Si lattice modes [16]. There is indication of absorption at 566 cm^{-1} which is attributed to the localized vibrational mode of C in Ge [17].

Fig. 5 shows a plot of PL intensity versus photon energy for two samples of SiGeC at low temperatures. With increasing C fraction, the peaks shift to higher energies. Although the mechanism for the SiGeC PL is not yet clear, there is a strong similarity of these peaks to the PL of SiGe alloys[18], and to previous reports of PL from SiGeC [9]. Furthermore, the high energy peaks (labeled NP) match the energies expected for the bandgaps at the measured compositions, and lie higher in energy than defect lines known for SiGe alloys [19]. Therefore we have attributed the peaks to exciton recombination without phonons (NP) and to the phonon replicas (labeled TO).

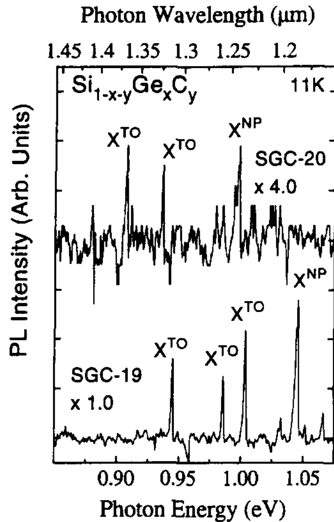

Fig. 5. Photoluminescence intensity versus photon energy for $Si_{0.08}Ge_{0.90}C_{0.02}$ (SGC-19) and $Si_{0.08}Ge_{0.91}C_{0.01}$ (SGC-20) measured at 11 K. Peaks shift higher in energy with C fraction and occur at higher energies than the known defect lines associated with SiGe alloys. Based on similarities to PL from SiGe alloys, the peaks were assigned to NP exciton recombination and phonon replicas.

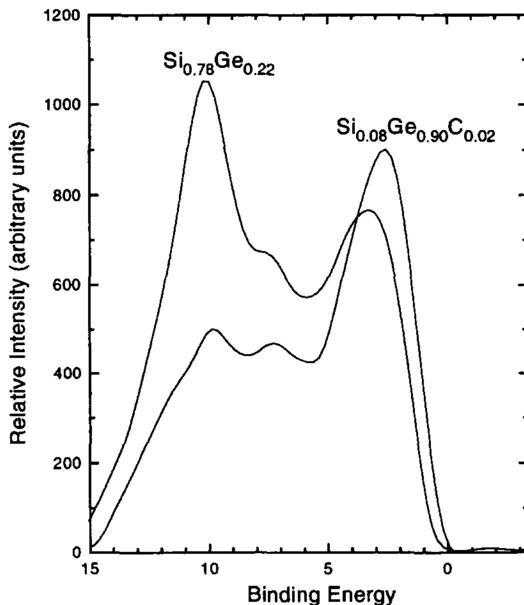

Fig. 6. Valence band density of states for $Si_{0.08}Ge_{0.90}C_{0.02}$ and for $Si_{0.78}Ge_{0.22}$, measured by XPS. The Si 2p core energy level was used as the reference for aligning the two spectra. The energy difference between valence band edges near 0 eV indicates the offset that would exist in a heterojunction between the two alloys. The binding energy is in eV.

4.3. Energy band offsets

Fig. 6 gives the energy distribution curves which are proportional to the valence band density of states (DOS) for a SiGeC alloy and a SiGe alloy, measured by XPS. The broad peaks are related to X and L critical point energies. The presence of C increases the valence band energy of the SiGeC alloys relative to SiGe alloys of similar composition. From the relative positions of the valence band edges and from the values for the bandgaps, we concluded that the energy band offsets of SiGeC alloys relative to Si were type II (staggered) heterostructures.

5. Conclusions

We have grown a series of $Si_{1-x-y}Ge_xC_y$ alloys by molecular beam epitaxy (MBE) and have performed a series of characterization measurements. The alloy were grown on (100) Si wafers at substrate temperatures from 400 to 600°C. Solid elemental sources were used for the Si and the Ge beams and a resistively heated graphite filament was used for the C beam. Reflection high energy electron diffraction measurements during growth indicated crystalline two dimensional layers. X-ray diffraction yielded the lattice constant which decreased with the C fraction. Optical transmission yielded the absorption coefficient versus photon energy. Photoluminescence at a temperature of 11 K showed a series of sharp peaks which shifted to higher energies with the C fraction. Using X-ray photoelectron spectroscopy, we measured the valence band energy of the alloys relative to Si. We found that the addition of C increases the valence band energy compared to SiGe alloys of similar composition.

Acknowledgements

This research was supported by AASERT grant F49620-92-J-0340, by AFOSR grant AFOSR-91-0371, by ONR grant N00014-93-1-0393, and by a grant from W.L. Gore and Associates. Special thanks to Dr. P.E. Thompson for secondary ion mass spectrometry, and to Dr. S.S. Iyer for providing the SiGe reference sample.

References

[1] K. Eberl, S.S. Iyer, S. Zollner, J.C. Tsang and F.K. LeGoues, Appl. Phys. Lett. 60 (1992) 3033.
[2] Z. Atzmon, A.E. Bair, E.J. Jaquez, J.W. Mayer, D. Chandrasekhar, D.J. Smith, R.L. Hervig and McD. Robinson, Appl. Phys. Lett. 65 (1994) 2559.
[3] G. He, M.D. Savellano and H.A. Atwater, Appl. Phys. Lett. 65 (1994) 1159.
[4] R.I. Scace and G.A. Slack, J. Chem. Phys. 30 (1959) 1551.
[5] J. Kolodzey, S. Zhang, P. O'Neil, E. Hall, R. McAnnally and C.P. Swann, Inst. Phys Conf. Ser. 137 (1993) ch.3, p. 357.
[6] R.A. Soref, Proc. IEEE 81 (1993) 1687.
[7] B. Dietrich, H.J. Osten, H. Rücker, M. Methfessel and P. Zaumseil, Phys. Rev. B 49 (1994) 17185.
[8] J. Kouvetakis, M. Todd, D. Chandrasekhar and D.J. Smith, Appl. Phys. Lett. 65 (1994) 2960.
[9] P. Boucaud, C. Francis, F.H. Julien, J.-M. Lourtioz, D. Bouchier, S. Bodnar, B. Lambert and J.L. Regolini, Appl. Phys. Lett. 64 (1994) 875.
[10] H.J. Osten, E. Bugiel and P. Zaumseil, J. Crystal Growth 142 (1994) 322.
[11] EPI MBE Products Group, St. Paul, MN, 1992.
[12] P.E. Thompson, M.E. Twigg, D.J. Godbey, K.D. Hobart and D.S. Simons, J. Vac. Sci. Technol. B 11 (1993) 1077.
[13] W. Zhu, B.R. Stoner, B.E. Williams and J.T. Glass, Proc. IEEE 79 (1991) 621.
[14] A.A. Demkov and O.F. Sankey, Phys. Rev. B 48 (1993) 2207.
[15] O. Madelung, M. Schulz and H. Weiss, Eds., Landolt–Börnstein, Numerical Data and Functional Relationships in Science and Technology, New Series, Vol. 17a, Section 1 (Springer, Berlin, 1982) p. 353.
[16] J.W. Strane, H.J. Stein, S.R. Lee, B.L. Doyle, S.T. Picraux and J.W. Mayer, Appl. Phys. Lett. 63 (1993) 2786.
[17] J.C. Tsang, K. Eberl, S. Zollner and S.S. Iyer, Appl. Phys. Lett. 61 (1992) 961.
[18] L.C. Lenchyshyn, M.L.W Thewalt, J.C. Sturm, P.V. Schwartz, E.J. Prinz, N.L. Rowell, J.-P. Noel and D.C. Houghton, Appl. Phys. Lett. 60 (1992) 3174.
[19] J. Michel, E.A. Fitzgerald, Y.-H. Xie, P.J. Silverman, M. Morse and L.C. Kimerling, J. Electron. Mater. 21 (1992) 1099.